

Latent attention on masked patches for flow reconstruction

Ben Eze¹[0009-0009-8594-082X], Luca Magri^{1,2}[0000-0002-0657-2611], and Andrea N3voa^{1,3}[0000-0003-0597-8326]

¹ Aeronautics Dept., Imperial College London, Exhibition Rd, London SW7 2BX, UK

² DIMEAS, Politecnico di Torino, Corso Duca degli Abruzzi, 24, Torino, 10129, Italy

³ I-X, Imperial College London, 84 Wood Lane, London W12 0BZ, UK
{ben.eze21,l.magri,a.novoa}@imperial.ac.uk

Abstract. Vision transformers have demonstrated outstanding performance on image generation applications, but their adoption in scientific disciplines, like fluid dynamics, has been limited. We introduce the *Latent Attention on Masked Patches* (LAMP) model, an interpretable regression-based modified vision transformer designed for masked flow reconstruction. LAMP follows a three-fold strategy: (i) partition of each flow snapshot into patches, (ii) dimensionality reduction of each patch via patch-wise proper orthogonal decomposition, and (iii) reconstruction of the full field from a masked input using a single-layer transformer trained via closed-form linear regression. We test the method on two canonical 2D unsteady wakes: a wake past a bluff body, and a chaotic wake past a flat plate. We show that the LAMP accurately reconstructs the full flow field from a 90%-masked and noisy input, across signal-to-noise ratios between 10 and 30 dB. Incorporating nonlinear measurement states can reduce the prediction error by up to an order of magnitude. The learned attention matrix yields physically interpretable multi-fidelity optimal sensor-placement maps. The modularity of the framework enables nonlinear compression and deep attention blocks, thereby providing an efficient baseline for nonlinear and high-dimensional masked flow reconstruction.

Keywords: Flow reconstruction · Vision Transformers · POD

1 Introduction

Reconstructing high-dimensional fields from sparse, noisy, and masked measurements is a central challenge in scientific machine learning and fluid mechanics [9, 21, 11]. In experimental settings, particle image velocimetry (PIV) measurements cover only a subset of the domain, and, since each run captures an independent realisation of the flow, PIV is often limited to mean-flow analyses rather than time-resolved full-field measurements in high-dimensional settings, e.g., [1]. To reconstruct full flow fields, data-driven approaches have been employed, such as convolutional neural networks (CNNs) [10, 12], generative adversarial networks [13], or graph neural networks [16], among many others. However, these

methods typically assume that a large fraction of the field is observed and are primarily designed for super-resolution, in-painting, or mean-flow reconstruction tasks. Real-time full-field reconstruction from sparse measurements can alternatively be achieved by coupling reduced-order models with data assimilation [5, 14]. Vision Transformers (ViTs) [6], in particular, have become the state-of-the-art backbone for image generation and large language models [15], but have not been fully adopted yet in the fluid dynamics community. Here, we introduce the *Latent Attention on Masked Patches* (LAMP) model, inspired by ViTs and masked autoencoders [8]. The key idea is to (i) partition each flow snapshot into non-overlapping patches; (ii) compress each patch into a low-dimensional latent representation; here, patch-wise Proper Orthogonal Decomposition (POD) [2]; and (iii) reconstruct the full field from a subset of the patches, i.e., a masked input, using an attention-based patch-to-patch prediction mechanism; here, implemented as a single-layer transformer trained via closed-form linear regression. This design guarantees convergence to a global minimum, eliminates dependence on learning-rate schedules and random weight initialisation, and yields fast, reproducible and physically interpretable results. Further, the modular architecture allows expressive components to be incorporated where performance demands it—such as nonlinear autoencoders [7, 17] or multi-layer transformers. The paper is structured as follows. Section 2 details the proposed LAMP. Section 3 demonstrates LAMP on two canonical unsteady wakes: a laminar bluff-body wake and a temporally chaotic wake. Section 4 closes the paper with conclusions and future work directions.

2 Latent Attention on Masked Patches (LAMP)

As illustrated in Fig. 1, LAMP consists of three stages: (i) data patching

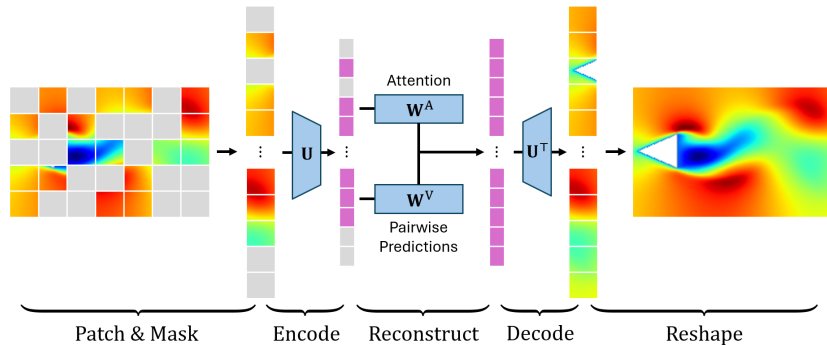


Fig. 1: Pictorial illustration of the patch-wise latent attention model (LAMP). A linear autoencoder embeds the input in a lower-dimensional latent space, where predictions can be made efficiently. The predictions are pair-wise (i.e., each patch predicts every other patch) and weighted with a confidence score.

and reshaping; (ii) patch-wise dimensionality reduction via linear autoencoding with proper orthogonal decomposition (POD); and (iii) attention-based patch-to-patch prediction in the latent space.

Patching. First, we divide the input 2D velocity data (of height H , width W and C components) $\mathbf{X}_{\text{in}} \in \mathbb{R}^{H \times W \times C}$ into N patches of dimension $D := CP^2$, which are flattened to obtain the *patched* data $\mathbf{X} \in \mathbb{R}^{N \times D}$ (see [6] for more details).

Patch-wise POD. We apply dimensionality reduction to compress \mathbf{X} into $\mathbf{Z} \in \mathbb{R}^{N \times N_e}$, with embedding (latent) dimension $N_e \ll D$. Each patch vector $\mathbf{x}_n \in \mathbb{R}^D$ is compressed into $\mathbf{z}_n \in \mathbb{R}^{N_e}$ by minimizing

$$\mathcal{L}^{\text{AE}} = \sum_{n=1}^N \|\tilde{\mathbf{x}}_n - \mathbf{x}_n\|_2^2, \quad \text{subject to } \tilde{\mathbf{x}}_n = \mathbf{U}_n \mathbf{U}_n^\top \mathbf{x}_n. \quad (1)$$

The patch-wise optimal orthonormal bases $\mathbf{U}_n \in \mathbb{R}^{D \times N_e}$ are obtained from the training timeseries as $\mathbf{X}_n^{\text{train}} \approx \mathbf{U}_n \boldsymbol{\Sigma} (\mathbf{V}_n^{\text{train}})^\top$, where the approximation arises as we retain only the first N_e leading singular vectors. Finally, we construct the encoding and decoding operators, \mathbf{E} and \mathbf{D} , as block-diagonal matrices composed of the patch-wise bases $\{\mathbf{U}_n\}_{n=1}^N$ such that

$$\mathbf{Z} = \mathbf{E}\mathbf{X}, \quad \text{and} \quad \tilde{\mathbf{X}} = \mathbf{D}\mathbf{Z}, \quad (2)$$

where the n -th block in \mathbf{E} and \mathbf{D} contain \mathbf{U}_n^\top and \mathbf{U}_n , respectively. The patched latent data \mathbf{Z} is then passed to the transformer. A low reconstruction loss \mathcal{L}^{AE} is a prerequisite for accurate masked predictions.

Masked prediction. We modify the attention equation presented in [20] for the task of single-layer reconstruction. The aim is to predict the full latent snapshot \mathbf{Z}^* from a masked input $\mathbf{Z}^{\text{masked}}$, where $Z_n^{\text{masked}} = -\infty$ for all masked indices $n \in \mathcal{N}_{\text{masked}}$. Each component in \mathbf{Z}^* is

$$Z_{me}^* = \sum_{n=1}^N \text{softmax}(\mathbf{a}_m)_n V_{mne}, \quad \text{for } \begin{cases} m = 1, \dots, N, \\ e = 1, \dots, N_e \end{cases} \quad (3)$$

where \mathbf{a}_m is the m -th row of the log-attention matrix $\mathbf{A} \in \mathbb{R}^{N \times N}$, and $\mathbf{V} \in \mathbb{R}^{N \times N \times N_e}$ is the value tensor; these are defined as

$$A_{mn} = \sum_{e=1}^{N_e} W_{mne}^{\text{A}} Z_{ne}^{\text{masked}}, \quad \text{and} \quad V_{mne} = \sum_{f=1}^{N_e} W_{mnef}^{\text{V}} Z_{nf}^{\text{masked}}, \quad (4)$$

where $\mathbf{W}^{\text{V}} \in \mathbb{R}^{N \times N \times N_e \times N_e}$ and $\mathbf{W}^{\text{A}} \in \mathbb{R}^{N \times N \times N_e}$ are the value and attention weight-tensors, which are trained on *unmasked* data with a two-step approach:

1. The value tensor \mathbf{W}^{V} can be viewed as an $N \times N$ grid of matrices: each block $\mathbf{W}_{mn}^{\text{V}} \in \mathbb{R}^{N_e \times N_e}$ defines a linear map that predicts patch \mathbf{z}_m from patch \mathbf{z}_n . These blocks are obtained by least-squares regression,

$$(\mathbf{Z}^{\text{train}})_m \approx \mathbf{W}_{mn}^{\text{V}}(\mathbf{Z}^{\text{train}})_n, \quad (5a)$$

where the corresponding linear prediction error is

$$\mathcal{L}_{mn}^{\text{lin}} = \|(\mathbf{Z}^{\text{train}})_m - \mathbf{W}_{mn}^{\text{V}}(\mathbf{Z}^{\text{train}})_n\|_2^2. \quad (5b)$$

2. The attention tensor \mathbf{W}^{A} is learned in a second stage and can be decomposed analogously, as a $N \times N$ grid of vectors $w_{mn}^{\text{A}} \in \mathbb{R}^{N_e}$. The error $\mathcal{L}_{mn}^{\text{lin}}$ provides a prediction uncertainty measure, so that predictions with lower $\mathcal{L}_{mn}^{\text{lin}}$ are assigned higher attention weights. In practice, we regress the *log-error*,

$$-\log(\mathcal{L}_{mn}^{\text{lin}}) \approx \mathbf{W}_{mn}^{\text{A}}(\mathbf{Z}^{\text{train}})_n. \quad (6)$$

At inference, the log-error is set to $-\infty$ for masked patches, before softmax converts the array into row-normalised attention values. Once \mathbf{Z}^{\star} is obtained, we test the LAMP architecture on unseen test data \mathbf{X}^{test} . The overall prediction error is defined as

$$\mathcal{L}^{\text{pred}} = \|\tilde{\mathbf{X}}^{\star} - \mathbf{X}^{\text{test}}\|_2^2 = \|\mathbf{D}\mathbf{Z}^{\star} - \mathbf{X}^{\text{test}}\|_2^2. \quad (7)$$

3 Results

We deploy the LAMP model to reconstruct the streamwise u and spanwise v velocity fields of two 2D unsteady wakes. First, we demonstrate the LAMP on the laminar wake of a triangular bluff body at Reynolds number $Re = 100$ [12], sampled at ~ 32 snapshots per shedding period; 100 snapshots are used for training and 60 for testing. Section 3.1 analyzes how performance depends on latent-space complexity, noise level, and patch placement. Second, we showcase the LAMP on a chaotic wake behind a flat plate at an angle of attack of 15° in Section 3.2, generated with an in-house solver based on [18] and comprising 2340 snapshots (~ 1377 Lyapunov times[19]), with 75% used for training and 20% for testing. We standardize both datasets by subtracting the temporal mean for each velocity field; the chaotic wake is additionally normalised element-wise by the standard deviation.

3.1 Laminar wake results

First, we validate the patch-wise POD and examine the loss \mathcal{L}^{AE} (Eq. 1), which sets the lower bound for the masked reconstruction error. Figure 2 shows that (1) \mathcal{L}^{AE} saturates rapidly with N_e , which is consistent with the well-known energy concentration of laminar bluff-body wakes into a few dominant POD modes; and (2) larger patches reach the same \mathcal{L}^{AE} at higher compression factors, which indicates that using very small patches may fragment the coherent vortex structures into features that carry little dynamical information.

Figure 3 shows the LAMP masked flow reconstruction results from randomly unmasked patches covering 10% of the domain for noise-free input (Fig. 3a) and

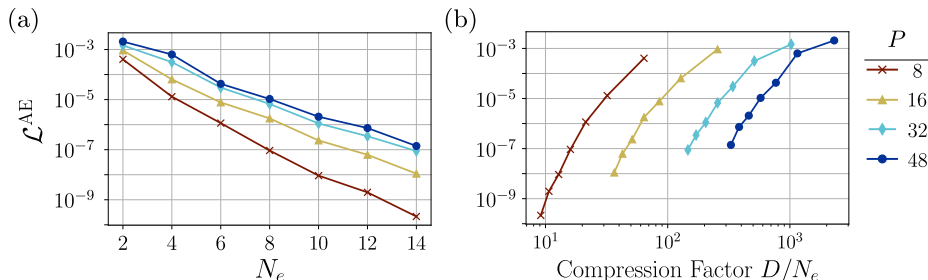


Fig. 2: Patch-wise POD reconstruction performance for varying patch size P . Loss \mathcal{L}^{AE} versus (a) latent dimension N_e and (b) compression factor D/N_e .

noisy input data (Fig. 3b-c). In the noise-free case, the LAMP provides flow-field reconstructions with prediction errors $\mathcal{L}^{\text{pred}}$ consistently lower than the variance of the added noise. Increasing the latent dimension N_e reduces $\mathcal{L}^{\text{pred}}$ (Fig. 3a), with larger patches outperforming smaller ones once sufficient modes are retained to resolve the coherent shedding. However, adding Gaussian noise to the masked input data such that $\mathbf{X}^{\text{noisy}} = \mathbf{X}^{\text{masked}} + \varepsilon$, where $\varepsilon \sim \mathcal{N}(0, \mathbf{P}_{\text{noise}})$, and $\mathbf{P}_{\text{noise}} = \mathbb{E}[\mathbf{X}^{\text{masked}}] \cdot 10^{-\text{SNR}/10}$, shifts the $\mathcal{L}^{\text{pred}}$ minima toward lower N_e (Fig. 3b-d). Small patches are less robust because their local POD bases amplify sub-patch-scale noise. In contrast, larger patches act as spatial filters that preserve the dominant flow structures. Notably, for moderate SNR a broad range of (P, N_e) yields $\mathcal{L}^{\text{pred}}$ below the noise variance σ_{noise}^2 (horizontal dashed lines). Therefore, the proposed LAMP successfully achieves simultaneous noise removal and flow reconstruction from masked data.

Next, we focus on the attention matrix, which yields as a by-product an interpretable method for sensor placement: the predictive-power maps shown in Fig. 4, which are computed by averaging the columns of $-\log \mathcal{L}_{mn}^{\text{lin}}$ (6) and reshaping into the physical space. Patches with highest predictive power are those whose local dynamics most accurately predict the rest of the field, i.e., the optimal sensor placement for reconstruction. Beyond reducing the resolution, increasing the patch size predominantly reduces the range of values in the attention map. By contrast, as N_e increases, high-power regions multiply from 1-2 near-body patches to distributed coverage across shear layers and far wake, mirroring the POD hierarchy. Placing sensors at persistent predictive-power peaks across N_e thus provides optimal multi-fidelity sensor layouts for both coarse and fine robust reconstructions.

3.2 Chaotic wake results

Because of the chaotic nature of the flow, the flat-plate wake requires larger patches and more POD modes than the laminar case, as shown in the prediction loss in Fig. 5a. We find that LAMP accurately captures the large-scale components of the flow, but underpredicts with regions of sharper gradients. Since the NavierStokes equations governing the flow dynamics are nonlinear, we may need

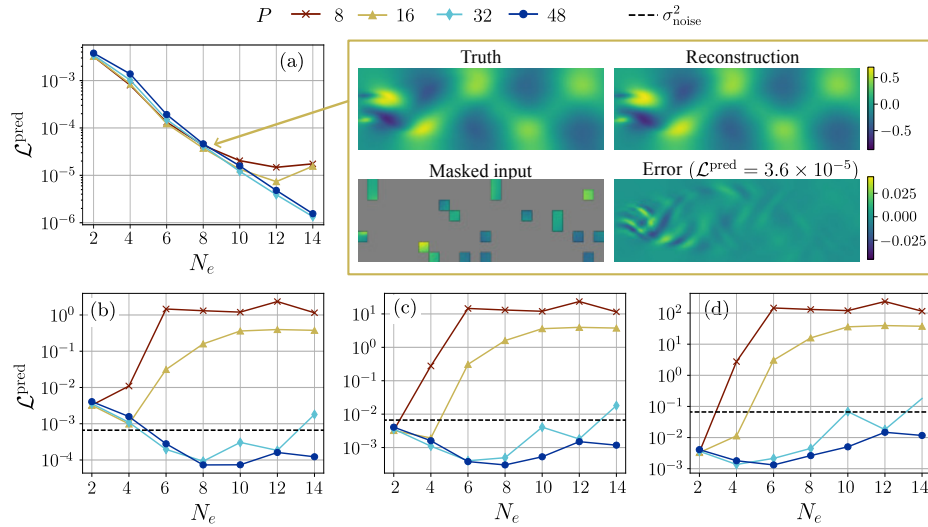


Fig. 3: Reconstruction error $\mathcal{L}^{\text{pred}}$ for varying noise levels, patch size P and latent dimension N_e . The input is noisy masked data $\mathbf{X}^{\text{masked}} + \varepsilon$, with SNR = (a) ∞ (noise-free), (b) 30 dB, (c) 20 dB, (d) 10 dB. The loss is computed against the noise-free target \mathbf{X}^{test} . Horizontal dashed lines show the noise variance σ_{noise}^2 . $\mathcal{L}^{\text{pred}}$ is calculated for 25 random patch arrangements and the *median* is plotted. An example reconstruction for the noise-free case with $P = 16$, $N_e = 8$ is shown.

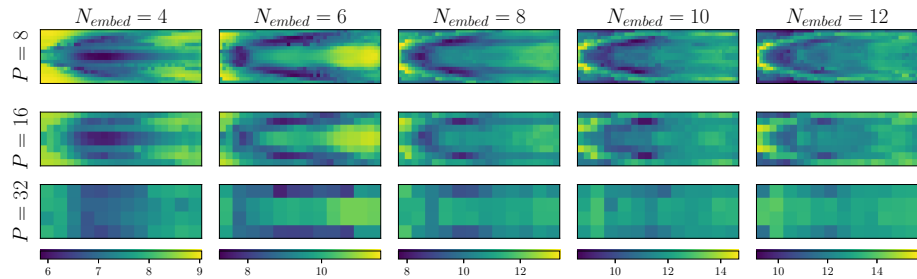


Fig. 4: Predictive-power maps for varying patch size and latent dimension. Patches with higher predictive power are better at predicting the full flow-field.

an infinite number of nonlinear measurement states to exactly reconstruct the flow field with a linear model [3, 4]. Adding the nonlinear observable uv , which physically relates to the turbulent shear stress, reduces $\mathcal{L}^{\text{pred}}$ by up to an order of magnitude for small patches (dashed vs solid lines in Fig. 5a). Figure 5b shows a reconstruction with $P = 48$, $N_e = 150$ for masked input on 3 channels (u, v, uv). This demonstrates the LAMP’s utility as a diagnostic for identifying effective measurement states (uv, u^2, v^2 , etc.) before deploying complex nonlinear autoencoders or deep transformer architectures.

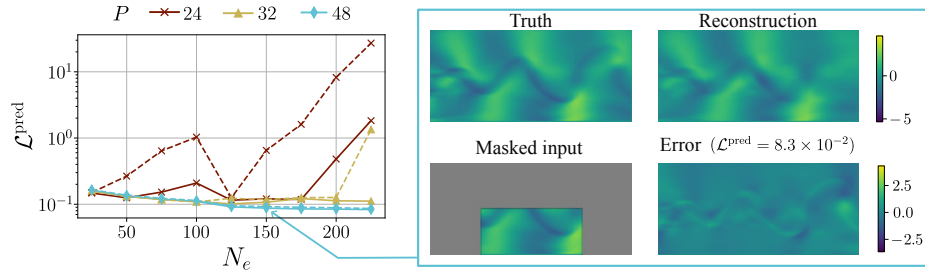


Fig. 5: Masked reconstruction on the chaotic wake. Prediction error $\mathcal{L}^{\text{pred}}$ for varying patch size and latent dimension with input channels (u, v) in dotted lines, and (u, v, uv) in solid lines. An example of the masked reconstruction from 2/8 unmasked patches with $P = 48$, $N_e = 150$, and three channels is shown.

4 Conclusion and future work

We introduce the *Latent Attention on Masked Patches* (LAMP) model, a regression-based architecture, inspired by Vision Transformers, designed to reconstruct high-dimensional flow fields from noisy and masked measurements. By integrating patch-wise Proper Orthogonal Decomposition with a linearly decomposable attention mechanism, we provide a framework that avoids hefty hyperparameter tuning and back-propagation. We showcase the LAMP on two test cases: a laminar wake past a triangular bluff body, and a chaotic wake past a flat plate. The LAMP has robust performance on the laminar wake, in which it successfully reconstructs flow fields from only 10% unmasked patches even when the input patches are corrupted by noise levels up to $\text{SNR} = 10$ dB. The reconstruction error remains an order of magnitude lower than the input noise variance, which shows that LAMP is both a reconstruction and de-noising tool. Beyond reconstruction, the attention maps from the LAMP provide an interpretable multi-fidelity sensor placement approach, which identifies the patches of highest importance for reconstruction. In the temporally chaotic wake, the LAMP maintains predictive accuracy, and we show that including additional input channels, such as the Reynolds stress component, can reduce error by up to an order of magnitude. This highlights the model’s utility in identifying effective measurement states. In future work, LAMP will be extended to include nonlinear autoencoding methods and multi-layered attention blocks.

Acknowledgments. LM acknowledges funding from ERC Starting Grant PhyCo 949388. AN is supported by the Eric and Wendy Schmidt AI in Science Fellowship.

References

1. Bekoglu, E., Bempedelis, N., Steiros, K.: Formation of turbulent secondary vortex street in absence of vortex shedding instability. *Journal of Fluid Mechanics* **1024**, A7 (2025)

2. Berkooz, G., et al.: The proper orthogonal decomposition in the analysis of turbulent flows. *Annual Review of Fluid Mechanics* **25**, 539–575 (1993)
3. Birkhoff, G.D., Koopman, B.O.: Recent contributions to the ergodic theory. *Proceedings of the National Academy of Sciences* **18**(3), 279–282 (1932)
4. Brunton, S.L., et al.: Modern koopman theory for dynamical systems. *SIAM Review* **42**(2), 229–340 (2022)
5. Cheng, S., Liu, C., Guo, Y., Arcucci, R.: Efficient deep data assimilation with sparse observations and time-varying sensors. *Journal of Computational Physics* **496**, 112581 (2024)
6. Dosovitskiy, A.: An image is worth 16 \times 16 words: Transformers for image recognition at scale. In: *Proceedings of the IEEE/CVF CVPR*. pp. 45–67 (2021)
7. Fukami, K., Fukagata, K., Taira, K.: Super-resolution reconstruction of turbulent flows with machine learning. *Journal of Fluid Mechanics* **870**, 106–120 (2019)
8. He, K., Chen, X., Xie, S., Li, Y., Dollár, P., Girshick, R.: Masked autoencoders are scalable vision learners. In: *Proceedings of the IEEE/CVF CVPR*. pp. 16000–16009 (2022)
9. Lam, R., Sanchez-Gonzalez, A., Willson, M., Wirnsberger, P., Fortunato, M., Alet, F., Ravuri, S., Ewalds, T., Eaton-Rosen, Z., Hu, W., et al.: Learning skillful medium-range global weather forecasting. *Science* **382**(6677), 1416–1421 (2023)
10. Lee, Y., Yang, H., Yin, Z.: Piv-dcnn: cascaded deep convolutional neural networks for particle image velocimetry. *Experiments in Fluids* **58**(12), 171 (2017)
11. Mo, Y., Magri, L.: Reconstruction of three-dimensional turbulent flows from sparse and noisy planar measurements: a weight-sharing neural network approach. *Data-Centric Engineering* **7**, e5 (2026). <https://doi.org/10.1017/dce.2026.10038>
12. Mo, Y., Traverso, T., Magri, L.: Decoder decomposition for the analysis of the latent space of nonlinear autoencoders with wind-tunnel experimental data (2024)
13. Nista, L., Pitsch, H., Schumann, C.D., Bode, M., Grenga, T., MacArt, J.F., Attili, A.: Influence of adversarial training on super-resolution turbulence reconstruction. *Physical Review Fluids* **9**(6), 064601 (2024)
14. Ózalp, E., Nóvoa, A., Magri, L.: Real-time forecasting of chaotic dynamics from sparse data and autoencoders. *Computer Methods in Applied Mechanics and Engineering* **450**, 118600 (2026)
15. Peebles, W., Xie, S.: Scalable diffusion models with transformers. In: *2023 IEEE/CVF International Conference on Computer Vision (ICCV)*. pp. 4172–4182. Paris, France (2023)
16. Quattromini, M., Bucci, M.A., Cherubini, S., Semeraro, O.: Mean flow data assimilation using physics-constrained graph neural networks. *Data-Centric Engineering* **6**, e48 (2025)
17. Racca, A., Doan, N.A.K., Magri, L.: Predicting turbulent dynamics with the convolutional autoencoder echo state network. *Journal of Fluid Mechanics* **975**, A2 (2023)
18. Stam, J.: Stable fluids. In: *Annual Conference on Computer Graphics and Interactive Techniques*. vol. 26, pp. 121–128 (1999)
19. Strogatz, S.H.: *Nonlinear Dynamics and Chaos: With Applications to Physics, Biology, Chemistry, and Engineering*. CRC Press (2018)
20. Vaswani, A., Shazeer, N., Parmar, N., Uszkoreit, J., Jones, L., Gomez, A.N., Kaiser, Ł., Polosukhin, I.: Attention is all you need. *Advances in neural information processing systems* **30** (2017)
21. Xia, C., Zhang, J., Kerrigan, E.C., Rigas, G.: Active flow control for bluff body drag reduction using reinforcement learning with partial measurements. *Journal of Fluid Mechanics* **981**, A17 (2024)